Temporal Apparent Diffusion Coefficient (ADC) Changes During Chemoradiation: An Imaging Biomarker for Tumour Response Monitoring and Spatial Recurrence Prediction in Glioblastoma

Daniel Moore-Palhares MDMSc , Liam SP Lawrence BEngMASc , Sten Myrehaug MD , James Stewart PhD , Jay Detsky PhDMD , Chia-Lin Tseng MDCM , Hanbo Chen MPHMD , Deepak Dinakaran MDPhD , Pejman Maralani MD , Mark Ruschin PhD , Beibei Zhang PhDFCCPM , James Perry MD , Mary Jane Lim-Fat MD , Arjun Sahgal MD , Hany Soliman MD , Angus Z Lau PhD

PII: S0360-3016(25)00260-3
DOI: https://doi.org/10.1016/j.ijrobp.2025.03.028
Reference: ROB 29315

To appear in: *International Journal of Radiation Oncology, Biology, Physics*

Received date: 13 September 2024
Revised date: 7 March 2025
Accepted date: 15 March 2025

Please cite this article as: Daniel Moore-Palhares MDMSc , Liam SP Lawrence BEngMASc , Sten Myrehaug MD , James Stewart PhD , Jay Detsky PhDMD , Chia-Lin Tseng MDCM , Hanbo Chen MPHMD , Deepak Dinakaran MDPhD , Pejman Maralani MD , Mark Ruschin PhD , Beibei Zhang PhDFCCPM , James Perry MD , Mary Jane Lim-Fat MD , Arjun Sahgal MD , Hany Soliman MD , Angus Z Lau PhD , Temporal Apparent Diffusion Coefficient (ADC) Changes During Chemoradiation: An Imaging Biomarker for Tumour Response Monitoring and Spatial Recurrence Prediction in Glioblastoma, *International Journal of Radiation Oncology, Biology, Physics* (2025), doi: https://doi.org/10.1016/j.ijrobp.2025.03.028

Title: Temporal Apparent Diffusion Coefficient (ADC) Changes During Chemoradiation: An Imaging Biomarker for Tumour Response Monitoring and Spatial Recurrence Prediction in Glioblastoma

Running Title: Spatial Recurrence Prediction in Glioblastoma

Authors: Daniel Moore-Palhares, MD, MSc[1*], Liam SP Lawrence, BEng, MASc[2*], Sten Myrehaug MD[1], James Stewart, PhD[1], Jay Detsky, PhD, MD[1], Chia-Lin Tseng, MDCM[1], Hanbo Chen, MPH, MD[1], Deepak Dinakaran MD, PhD[1], Pejman Maralani, MD[3], Mark Ruschin, PhD[1], Beibei Zhang, PhD, FCCPM[1], James Perry, MD[4], Mary Jane Lim-Fat, MD [4], Arjun Sahgal, MD[1], Hany Soliman MD[1#], Angus Z Lau, PhD[5#]

* Co-first authors, contributed equally

# Co-senior authors, contributed equally

Affiliations:

1. Department of Radiation Oncology, Odette Cancer Centre, Sunnybrook Health Sciences Centre, University of Toronto, Toronto, Ontario, Canada
2. Department of Medical Biophysics, University of Toronto, Toronto, ON, Canada,
3. Department of Medical Imaging, Sunnybrook Health Sciences Centre, University of Toronto, Toronto, Ontario, Canada

4. Division of Neurology, Department of Medicine Sunnybrook Health Sciences Centre, University of Toronto, Toronto, ON, Canada.
5. Department of Physical Sciences, Sunnybrook Research Institute, University of Toronto, Toronto, ON, Canada

Corresponding author:

Dr. Angus Z Lau, PhD

Department of Physical Sciences, Sunnybrook Research Institute, University of Toronto, Toronto

2075 Bayview Ave, M4N 3M5, Toronto, ON, Canada.

Telephone: (+1) 416-480-6100, ext. 685480

Email: angus.lau@sri.utoronto.ca

Statistical analysis: Liam SP Lawrence, BEng, MASc

Conflict of Interest/Disclosures: D.M.P: none; **L.S.P.L**.: Travel expenses/accommodations from Elekta AB; **S.M.:** none; **J.S.:** none; **J.D.:** none; **C.L.T**: has received travel accommodations/expenses & honoraria for past educational seminars by Elekta, belongs to the Elekta MR-Linac Research Consortium, and is an advisor/consultant with Abbvie.**; H.C.:** none; **D.D.:** none; **P.M.:** none; **M.R.:** coinventor of and owns associated intellectual property specific

to the image guidance system on the Gamma Knife Icon; **B.Z.:** none; **J.P.:** none; **M.J.L.F.:** none; **A.S.:** Elekta/Elekta AB: Research grant, Consultant, Honorarium for past educational seminars, Travel Expenses, Varian: Honorarium for past educational seminars, BrainLab: Research grant, Consultant, Honorarium for educational seminars, Travel Expenses, AstraZeneca: Honorarium for educational seminars, ISRS: President of the International Stereotactic Radiosurgery Society (ISRS), Seagen Inc: Honorarium for education seminars and research grants, Cerapedics: Honorarium for educational seminars, Travel Expenses, CarboFIX: Honorarium for educational seminars, Servier: Honorarium for educational seminars; **H.S.:** none; **A.Z.L.:** none

Funding: This study was funded by the Department of Radiation Oncology, Sunnybrook Odette Cancer Centre, Natural Sciences and Engineering Research Council (RGPIN-2017-06596, CGS-D program), Ontario Early Researcher Awards Program, and Canadian Institutes of Health Research (CIHR 175081).

Data Availability: Research data are stored in an institutional repository and will be shared upon request to the corresponding author.

Acknowledgments: We express our gratitude to all the patients, family members, and participating staff from Sunnybrook Health Sciences Centre for their valuable contributions to this study. Additionally, we gratefully acknowledge funding from the following

sources: Department of Radiation Oncology, Sunnybrook Odette Cancer Centre, Natural Sciences and Engineering Research Council (RGPIN-2017-06596, CGS-D program); Ontario Early Researcher Awards Program; Canadian Institutes of Health Research (CIHR 175081).

Authorship statement: Conception and design: D.M.P., L.S.P.L., S.M., A.S., H.S., A.Z.L.; **Acquisition of data**: D.M.P., L.S.P.L., S.M., J.S.; **Data analysis**: L.S.P.L.; **Interpretation of the results**: D.M.P., L.S.P.L., H.S., A.Z.L.; **Writing:** D.M.P., L.S.P.L., H.S., A.Z.L.; **Review, and/or revision of the manuscript**: D.M.P., L.S.P.L., S.M., J.S., J.D., C.L.T., H.C., D.D., P.M., M.R., B.Z., J.P., M.J.L.F., A.S., H.S., A.Z.L. **Study supervision**: H.S., A.Z.L.

Word count: Abstract = 248; Total manuscript word count = 4350.

Abstract

Background: Apparent diffusion coefficient (ADC) from diffusion-weighted imaging (DWI) has been shown to detect early treatment response in glioblastoma. This prospective observational serial imaging study aimed to compare apparent diffusion coefficient (ADC) changes in gross tumour volume (GTV) regions that developed recurrence versus those that remained recurrence-free.

Methods: Patients with glioblastoma underwent DWI at radiation planning (baseline, Fx0), fraction 10 (Fx10), fraction 20 (Fx20), and 1 month after completing a 6-week course of chemoradiation (P1M). Recurrence was contoured at the earliest magnetic resonance imaging

(MRI) showing progression. The intersection of the GTV and recurrence was labelled resistant-GTV, while non-intersecting GTV was labelled sensitive-GTV. ADC values and percentage changes from Fx0 were compared between these regions.

Results: Eighty patients were analyzed. Median absolute ADC values for resistant (0.94 μm^2/ms, interquartile range [IQR]: 0.84, 1.08) and sensitive GTV (0.93 μm^2/ms, IQR: 0.87, 1.13) were similar at baseline (P=0.193), but statistically significant differences were observed from the start of radiotherapy. Median ADC changes from baseline for resistant- and sensitive-GTV were +2.5% vs. +15.1% at Fx10 (P<0.001), +8.1% vs. +23.1% at Fx20 (P<0.001), and +21.2% vs. +36.4% at P1M (P<0.001), respectively. Smaller ADC changes at Fx10 (odds ratio [OR] 0.95, P=0.005) and Fx20 (OR 0.95, P=0.010) were independent predictors of increased risk of GTV failure, adjusting for MGMT promoter methylation and extent of surgical resection.

Conclusions: Temporal ADC changes are promising imaging biomarkers for treatment response and spatial recurrence prediction, and may provide a target for MRI-guided biologically adapted radiation clinical trials.

Keywords: glioblastoma, diffusion-weighted imaging, apparent diffusion coefficient, imaging biomarker, spatial recurrence prediction

Introduction

Glioblastoma is the most common and aggressive primary brain tumour (1). Despite intensive local treatment, including maximal safe surgical resection and adjuvant chemoradiation, 85-90% of failures occur within the high-dose volume (2). In an effort to enhance local control and consequently improve survival, clinical trials have explored increasing the radiation dose to the contrast-enhanced gross tumour volume (GTV); however, this approach has not yielded improved outcomes (3–7). Subsequent trials shifted focus to using baseline (i.e. pre-treatment) functional imaging to guide dose-escalation targets (8–14), as these modalities provide information on tumour biology and aggressiveness (13–17). Small single-arm trials using positron emission tomography (PET), diffusion-weighted imaging (DWI), and/or magnetic resonance spectroscopic imaging (MRSI) demonstrated a reduction in the risk of in-field failure (12) and improved survival with dose escalation compared to historical controls (11–13). However, the randomized phase 3 SPECTRO GLIO trial, which increased the dose to 72 Gy in 30 fractions using MRSI metabolic abnormalities, failed to demonstrate improved outcomes over the standard regimen (10). These data suggest that while the benefit of delivering doses beyond 60 Gy in 30 fractions remains unproven, the optimal target for dose-escalation strategies is still unknown.

The integration of magnetic resonance imaging (MRI) scanners into radiation treatment machines (known as MRI linear accelerator [MR-Linac]) offers new opportunities to utilize repeated MRI during treatment, rather than just baseline imaging, for designing novel boost strategies. We previously conducted a prospective observational study in which patients with glioblastoma underwent MRI before, during, and after standard concurrent chemoradiation (18–

20). This work has laid the groundwork for ongoing phase II clinical trials (18,19,21), which are evaluating the efficacy and safety of intelligently reducing the treatment volume with weekly anatomical adaptation on the MR-Linac (ClinicalTrials identifier: xxxxxx, xxxxxx). Additionally, mid-treatment multiparametric MRI was performed to investigate biological changes secondary to radiotherapy and identify imaging biomarkers of treatment response, aiming to develop future MRI-guided, biologically-adapted clinical trials. Among the functional sequences acquired, DWI is of special interest as it is sensitive to changes in tumour cellularity (22–26). DWI assesses the movement of water molecules within tissues, and the degree of water diffusion is quantified by the apparent diffusion coefficient (ADC). ADC is inversely correlated with tumour cellularity: in highly cellular tumours, the movement of water molecules is restricted, resulting in low ADC values (25,26). As radiotherapy induces tumour cell death, tissue becomes less restrictive, and ADC values are expected to increase throughout the treatment (22).

Previous studies showed that changes in tumour ADC during radiotherapy can provide early detection of therapeutic effects and are prognostic for progression-free and overall survival in glioblastoma (20,27–30). This evidence supports the use of DWI for monitoring temporal response and predicting time to treatment failure. Building on these findings, we speculate that changes in tumour ADC could also monitor spatial responses and identify potential sites of tumour recurrence, which could guide adaptive dose-escalation targets. Given that most failures occur in-field within the GTV, either as progression of the existing tumour or recurrence in the surgical cavity, we focused on predicting spatial GTV recurrence (2). We hypothesize that GTV regions that subsequently develop recurrence exhibit smaller reductions in cellularity and smaller ADC increases during treatment compared to those regions that do not recur. To test this

hypothesis, we conducted an innovative pattern of failure analysis by geographically separating the GTV into areas that eventually developed recurrence versus areas that remained recurrence-free, and comparing the ADC changes across these progressive and responsive subregions.

Methods

Study Cohort

This prospective observational serial imaging study enrolled patients with newly diagnosed contrast-enhancing glioblastoma according to the 2016 World Health Organization (WHO) classification. All patients underwent biopsy or maximal safe resection and were planned for a six-week course of conventionally fractionated radiotherapy with concurrent and adjuvant temozolomide chemotherapy. The study involved the acquisition of multiparametric MRI, including DWI, at four time points: radiotherapy planning (baseline, Fx0), fraction 10 (Fx10), fraction 20 (Fx20), and one month after radiotherapy completion (P1M) (Figure 1A). For the purpose of this recurrence prediction study, we included only those who had DWI at Fx0 and at least one additional time point during concurrent chemoradiation. We excluded patients who fell into the following categories: a prior history of low-grade glioma, discontinuation of radiotherapy, poor registration of tumour/cavity and recurrence, clinical deterioration or death without evidence of radiological progression, and insufficient follow-up to confidently map tumour recurrence (further detailed below). The study was approved by the xxxxxx research ethics committee (project ID: xxxxxx), and all participants provided written consent.

Treatment Details and Follow-up

Patients were simulated with computed tomography (CT) and planning MRI (Fx0) (31). The GTV was contoured on the T1-weighted contrast-enhanced (T1c) imaging and it consisted of the surgical resection cavity and any residual enhancing tumour, following contouring guidelines (32). The clinical target volume (CTV) was defined by a 1.5 cm isotropic expansion of the GTV, adjusted per natural anatomical boundaries, and further expanded by 4 mm isotropically to create the planning target volume (PTV). Patients were intended to receive 60 Gy in 30 fractions, but a dose reduction to 54-56 Gy was allowed if there were concerns about toxicity, such as large tumour size or brainstem involvement. Patients received standard non-adaptive radiation therapy. Treatment was administered using intensity-modulated radiation therapy (IMRT) or volumetric arc therapy (VMAT) with CT-guided or 1.5 T MRI-guided Elekta linear accelerators (Elekta AB, Stockholm, Sweden). Temozolomide was concurrently administered with radiation at a daily dose of 75 mg/m² of body surface area throughout the radiotherapy period, followed by six cycles of adjuvant treatment at 200 mg/m² once daily for the first five days of each 28-day cycle, as tolerated. Patients were followed per our institutional protocol with diagnostic contrast-enhanced MRI of the brain every 4–8 weeks, or sooner if clinically indicated.

Data Collection, MR Imaging, and delineation of regions of interest

Demographic, tumour, and treatment characteristics were collected from electronic medical records and radiotherapy treatment planning system, including age at diagnosis, tumour location, extent of surgical resection (biopsy, subtotal resection [STR], gross total resection [GTR]), isocitrate dehydrogenase (IDH) mutation and O6-methylguanine DNA

methyltransferase (MGMT) promoter methylation status, Eastern Cooperative Oncology Group (ECOG) performance status, and radiotherapy dose.

The serial multiparametric MRI scans were acquired at the aforementioned time points (Fx0, Fx10, Fx20, P1M) using a dedicated 1.5 or 3.0 T MRI simulation scanner (Ingenia or Achieva, Philips Healthcare, Amsterdam, Netherlands)(31). DWI was acquired with diffusion encoding along three perpendicular directions, and a trace image was created. Select protocol parameters are shown in Supplementary Table 1. ADC maps were generated to provide a visual and quantitative representation of in vivo diffusivity by fitting the data on a voxel-by-voxel basis using linear least-squares fitting to the log-signal decay versus the b-value. All b-values in the range of 0 to 1000 s/mm² were used.

The diagnostic follow-up MRIs until the last follow-up were reviewed, and radiological recurrence was defined at the earliest time point showing contrast-enhancing progression according to the Response Assessment in Neuro-oncology (RANO) 2.0 criteria for enhancing tumours (33). Specifically, if non-measurable enhancing disease (<10mm x 10mm) was confirmed to be progressive disease on subsequent scans, the date of progression was backdated to when the concern for progression was first raised (33).

For study purposes, radiation oncologists with over 5 years (xxxxxx) and 10 years (xxxxxx) of experience retrospectively contoured the regions of interest while being blinded to the DWI MRI and ADC maps. The regions of interest included the GTV and the interior of the resection cavity contoured on the T1c MRI at each time point (Fx0, Fx10, Fx20, P1M), and the contrast-enhancing recurrence contoured at the earliest T1c MRI showing tumour progression (Figure 1B). The GTV was contoured per guidelines as previously described (32). For each

patient, the T1c image at Fx0 was chosen as the reference image. All other images, including T1c at Fx10, Fx20, and P1M, ADC maps at Fx0, Fx10, Fx20, and P1M, and T1c at recurrence, were co-registered and aligned to T1c at Fx0 using rigid registration(34,35), and the contours were propagated to the reference image.

Analysis of ADC Values Stratified by the Pattern of Failure

The pattern of failure was defined clinically upon review of all follow-up MRI scans, aiming to identify specific areas of the GTV that could be confidently labeled as either sensitive (areas that remained recurrence-free) or resistant (areas that developed recurrence) to chemoradiation. Three distinct patterns of GTV recurrence were identified: 1) "Entire GTV Failure," where the entire GTV recurred and a well-defined recurrence-free sub-volume could not be identified; 2) "Partial GTV Failure," where a well-defined GTV sub-volume remained free of recurrence until the last follow-up while another part of the GTV progressed; and 3) "No GTV Failure," where patients did not experience recurrence in the GTV until the last follow-up and were followed for at least 20 months. We excluded from the analysis patients with partial GTV failure who died soon after progression without a confirmatory MRI scan, and those with no GTV failure who were followed for less than 20 months, as these cases represent insufficient follow-up to confidently confirm the absence of failure in areas labeled sensitive to chemoradiation.

Among patients with partial GTV failure, the regions of the GTV that intersected with the recurrence were labeled "Resistant-GTV" (R-GTV), while the regions that did not intersect were

labeled "Sensitive-GTV" (S-GTV). For patients with entire GTV failure, the entire GTV volume was labeled R-GTV, while for those with no GTV failure, the entire GTV was labeled as S-GTV (Figure 1C).

For each patient, the absolute ADC values within the R-GTV and S-GTV, as applicable, were measured at each time point (Fx0, Fx10, Fx20, and P1M), excluding the interior of the surgical cavity to avoid ADC measurement bias (Figure 1D). The relative (%) ADC change at Fx10, Fx20, and P1M was computed for R-GTV and S-GTV regions, using Fx0 (baseline) as the reference.

Study Outcomes

The primary endpoint was to compare changes in ADC values between the R-GTV and S-GTV. The secondary endpoint was to correlate ADC changes with time to GTV failure and identify predictive factors for spatial GTV recurrence.

Statistical analyses

Descriptive data were presented as counts and percentages for categorical variables and as medians with ranges or interquartile ranges (IQR) for continuous variables. The chi-square test compared categorical characteristics and one-way analysis of variance (ANOVA) compared continuous variables between the patient cohorts (entire, partial, or no GTV failure). Absolute ADC values or relative (%) ADC changes were compared between R-GTV and S-GTV at each timepoint. Analyses were on a per-GTV sub-volume basis, with ADC measurements taken separately from R-GTV and S-GTV regions for patients experiencing partial GTV failure. An unpaired two-sided t-test hypothesized that absolute ADC values or relative (%) changes would

differ between the R-GTV group and the S-GTV group. A mixed-effects linear model evaluated relative ADC changes using all data at Fx10, Fx20, and P1M. Fixed effects were GTV response (R-GTV or S-GTV), the time in weeks since treatment start, and their interaction. Random effects were subjects (i.e., each subject had a unique intercept). A paired two-sided t-test compared R-GTV and S-GTV sub-volumes for the partial GTV failure cohort (i.e., between sub-volumes for the same patients); and an unpaired two-sided t-test compared ADC changes between entire GTV failure and partial GTV failure (R-GTV sub-volume) or between no GTV failure and partial GTV failure (S-GTV sub-volume). The concordance index was computed between the relative ADC change at each timepoint and the time to GTV failure, defined as the duration from surgical resection to the earliest MRI showing progression within the GTV. Patients/sub-volumes were stratified by time to GTV failure using a clinically defined threshold of 12 months (R-GTV, ≤12 months; R-GTV, >12 months; S-GTV, no failure), and the relative ADC change was compared between groups with ANOVA. Logistic regression predicted the probability of GTV recurrence (R-GTV) based on ADC values or change at either Fx10 or Fx20 and clinical factors including MGMT methylation status, IDH mutation status, age, sex, tumour location, extent of resection, radiation dose, and ECOG status. Stepwise model selection with backward variable search created a minimal model by the Akaike information criterion. An exploratory model with relative ADC change at Fx10 and Fx20 alone was constructed, and model selection determined which would yield a superior predictor. All P values were 2-sided, with statistical significance defined as $P < .05$. All statistics used R version 4.1.2 (R Core Team, Vienna, Austria). The logistic model selection used the stepAIC function in the MASS package(36).

Results

A total of 129 patients with glioblastoma were enrolled in the original serial imaging study, of which 107 comprised the DWI cohort. Twenty-seven patients were further excluded for reasons detailed in the cohort diagram (Figure 2), resulting in a final cohort of 80 patients. All 80 patients had DWI at Fx0 and Fx10, 79 (99%) at Fx20, and 76 (95%) at P1M. Patients were enrolled between November 2017 and April 2021 and followed until March 2024. The median interval from Fx0 to radiation treatment start was 7 days (range, 2-16). The median follow-up interval from surgical resection for the entire cohort was 48.4 months (range, 4.3-64.5).

Table 1 summarizes the characteristics of the studied population, stratified by the pattern of failure. The median age of the entire cohort was 54 years (range, 19-75) and most patients had an ECOG performance status 0-1 (75%, n=60/80), had undergone subtotal resection (STR) (54%, n=43/80), were IDH wildtype (96%, n=77/80), MGMT promoter unmethylated, (53%, n=42/80), and treated with 60 Gy in 30 fractions (80%, n=64/80). Forty-nine patients (61%, n=49/80) experienced entire GTV failure, 14 patients (18%, n=14/80) developed partial GTV failure, and 17 patients (21%, n=17/80) had no GTV failure. Among those patients with no GTV failure, 6 recurred within the CTV and/or T2/FLAIR hyperintensity, 4 recurred outside the CTV, and 7 were alive and free of recurrence. The cohorts of patients with partial and no GTV failure had a higher proportion of individuals who underwent GTR (p=0.049), had MGMT promoter methylated (p=0.005), and completed 6 cycles of adjuvant temozolomide (p<0.001) as compared to those with entire GTV failure. For patients with partial GTV failure, the fraction of the GTV occupied by the recurrence (R-GTV) had a median value of 26% (range, 3–62%).

Absolute ADC values and temporal ADC changes for the entire cohort

At baseline (Fx0), the median absolute ADC values for R-GTV and S-GTV were similar: 0.94 μm^2/ms (IQR: 0.84-1.08) vs. 0.93 μm^2/ms (IQR: 0.87-1.13), respectively (P=0.387) (Figure 3A). However, with the initiation of chemoradiation, statistically significant differences in median ADC values between R-GTV and S-GTV emerged: 1.00 μm^2/ms (IQR 0.88, 1.13) vs. 1.12 μm^2/ms (IQR 1.00, 1.35) at Fx10 (P=0.002), 1.06 μm^2/ms (IQR 0.95, 1.21) vs. 1.16 μm^2/ms (IQR 1.03, 1.44) at Fx20 (P=0.003), and 1.20 μm^2/ms (IQR 1.06, 1.33) vs. 1.38 μm^2/ms (IQR 1.22, 1.57) at P1M (P<0.001), respectively.

The median ADC change from baseline (Fx0) for R-GTV and S-GTV was +2.5% (IQR -2.7, 14.9) vs. +15.1% (IQR 8.2, 27.8) at Fx10 (P=0.001), +8.1% (IQR -0.8, 23.3) vs. +23.1% (IQR 16.4, 28.6) at Fx20 (P=0.001), and +21.2% (IQR 10.2, 35.6) vs. +36.4% (IQR 25.3, 52.6) at P1M (P=0.001), respectively (Figure 3B). A linear mixed-effects model revealed a statistically significant difference in temporal ADC changes between R-GTV and S-GTV (P<0.001). The interaction term (tumour response: weeks) was not statistically significant (P=0.362), indicating that most differences between R-GTV and S-GTV manifested by radiotherapy Fx10.

Temporal ADC changes stratified by subgroups

ADC changes for R-GTV and S-GTV were compared across the three patterns of failure cohorts (entire GTV, partial GTV, and no GTV failure) (Figure 3C and Supplementary Figure 1). Among patients with partial GTV failure, R-GTV subregions exhibited statistically significant smaller ADC changes at all time points compared to S-GTV: 0% (IQR: -1.7, 10.4) vs +15.3% (IQR: 12.8, 25.9) at Fx10 (P=0.007), +6.9% (IQR: 3.7, 18.3) vs +24.8% (IQR: 18.1, 29.0) at Fx20 (P=0.002), and +19.5 (IQR: 10.4, 26.9) vs +37.3% (IQR: 21.1, 60.2) at P1M (P=0.002). An

individual patient analysis revealed that 13 out of 14 patients (93%) with partial GTV failure had a smaller ADC increase in the R-GTV compared with the S-GTV (Supplementary Figure 2). Among all R-GTV regions, there was no significant difference in percentage ADC changes between those originating from entire GTV failure and those from partial GTV failure (P=0.91 at Fx10, P=0.92 at Fx20, and P=0.25 at P1M). Similarly, among all S-GTV regions, no significant difference was observed in ADC changes between those originating from patients with no GTV failure and those from partial GTV failure (P=0.67 at Fx10, P=0.40 at Fx20, and P=0.61 at P1M).

A significant correlation was observed between ADC change and time to GTV recurrence, with a concordance index of 0.60 (95% CI 0.54, 0.66, P<0.001) at Fx10, 0.60 (95% CI 0.53, 0.66, P=0.003) at Fx20, and 0.58 (95% CI 0.51, 0.64, P=0.015) at P1M. Regions of R-GTV were stratified by time to failure (from surgical resection) using a clinically defined threshold of 12 months and compared with S-GTV. The median ADC change at Fx10, Fx20 and P1M was +1.5% (IQR: -4.1, 14.4), +7.9% (IQR: -1.9, 22.0), and +21.6% (IQR: 10.1, 37.5) for R-GTV regions progressing earlier than 12 months, versus +10.2% (IQR: -0.2, 17.1), +17.3% (IQR: 5.6, 25.6), and +19.9% (IQR: 15.2, 31.4) for those progressing after 12 months, and +15.1% (IQR: 8.2, 27.8), +23.1% (IQR: 16.4, 28.6), and +36.4% (IQR: 25.3, 52.6) for GTV regions with no progression (S-GTV) (Figure 3D). From the one-way ANOVA, the p-values for comparisons were statistically significant at all time points (P<0.001 at Fx10, P=0.002 at Fx20, and P=0.007 at P1M). Examples of temporal ADC changes in patients with different patterns of failure are shown in Figure 4.

Predictive Factors for GTV Recurrence

Two separate logistic regression models were constructed, each incorporating ADC change at either Fx10 or Fx20 along with suspected predictive factors as detailed in the methods. Multivariable analysis identified smaller changes in ADC values at Fx10 (odds ratio [OR] 0.95, 95% CI 0.91-0.98, P=0.005) and Fx20 (OR 0.95, 95% CI 0.92-0.99, P=0.010), MGMT promoter unmethylation (OR 4.4, 95% CI 1.5,14.0, P=0.009 for Fx10; OR 4.3, 95% CI 1.5-14.0, P=0.010 for Fx20), and non-GTR (OR 22.7, 95% CI 2.8-526.3, P=0.012 for Fx10; OR 20.4, 95% CI 2.6-476.2, P=0.014 for Fx20) as independent predictors of increased risk of GTV failure (Supplementary Table 2). Absolute ADC values at Fx10 (P=0.800) and Fx20 (P=0.702) were not predictive of spatial recurrence. An exploratory bivariate analysis including ADC change at both Fx10 and Fx20 showed the change at Fx10 remained statistically significant (OR 0.95, 95% CI 0.92-0.98, P=0.002), indicating its superior relevance for prediction. Figure 5 illustrates the probability of GTV recurrence based on relative ADC change at Fx10 and Fx20, MGMT promoter methylation status, and extent of surgical resection.

Discussion

This is the largest prospective multifunctional serial imaging study conducted for glioblastoma and the first to show that percentage ADC changes during radiotherapy are independent predictors of spatial GTV recurrence. We observed a significant correlation between ADC change and time to GTV recurrence, with regions that recurred earlier showing smaller ADC increases compared to those with longer recurrence times. This study provides evidence of the utility of DWI as a tool for monitoring early spatial treatment response and identifying tumour regions resistant to chemoradiation.

We identified no difference in baseline ADC values between resistant and sensitive GTV regions, suggesting that pre-treatment measurement alone may not be accurate for predicting geographic recurrence. Instead, the rate of ADC change in response to radiation emerged as a critical biomarker. We speculate that pre-treatment values reflect cellular density and tumour proliferation outside the selective pressure of treatment, whereas mid-treatment changes provide biological information on tumour chemoradiosensitivity, revealing areas less responsive to treatment and at higher risk of recurrence. This contrasts with previous studies that suggested the utility of pre-treatment DWI for predicting recurrence locations in glioblastoma, with findings showing that 45-88% of baseline ADC abnormalities overlap with recurrent tumour sites (15–17). This should be considered in the context that most tumours recur in-field and a high overlap rate would be expected regardless of the use of multiparametric imaging (2,37), while our data is supported by a statistical comparison of ADC values between GTV regions that progressed versus those that remained recurrence-free. Moreover, our exploratory analysis (Supplementary Figure 3) revealed dependency of baseline ADC on the extent of surgical resection, with biopsied tumours (median ADC 0.88 μm^2/ms, IQR: 0.82, 0.95) having significantly lower values compared to completely resected ones (median ADC 0.99 μm^2/ms, IQR: 0.89, 1.19, p=0.03). This indicates that pre-treatment ADC may be subject to selection bias. In contrast, temporal ADC changes are unlikely to be influenced by surgical resection or imaging acquisition protocols, as they use the patient's own baseline imaging features as a reference, potentially providing more reliable and generalizable data across different institutions than baseline values.

We observed that GTV regions progressing within 12 months exhibited smaller ADC increases than those progressing later, which in turn showed smaller changes than regions that did not progress until the last follow-up. This continuous spectrum suggests that greater tumour

cell kill (for which ADC change is a surrogate) results in longer times to GTV recurrence, or in some cases no local failure at all. Moreover, we identified that most differences in ADC change between R-GTV and S-GTV manifested at the second week of treatment, allowing for early identification and potential treatment adaptations during the radiotherapy course. These findings align with our previous analyses, which demonstrated that those with a greater reduction in the volume of low-ADC (hypercellular) tumour during radiation had longer progression-free and overall survival, with statistical significance emerging in the second week of treatment (20). Furthermore, our results align with those of Mohamed et al. (38), who studied serial DWI imaging in head and neck cancer patients undergoing radiotherapy. They found that patients with mid-treatment tumour ADC changes greater than 7% had improved local control and recurrence-free survival compared to those with smaller changes. Additionally, a similar sub-volume analysis to ours revealed significant differences in mid-treatment ADC changes between primary GTV regions that progressed versus those that responded to treatment. Furthermore, their results indicated that baseline DWI parameters were not prognostic for clinical outcomes; instead, dynamic ADC changes in response to radiation served as a key imaging biomarker (38).

Our study revealed significant spatial response heterogeneity in glioblastomas. This finding is supported by previous transcriptomics studies, which mapped the distribution of tumour cells within the glioblastoma microenvironment and revealed substantial genetic and molecular differences across tumour subregions (39–41). These intratumoural disparities may explain why different regions within the same tumour may contain treatment-sensitive or treatment-resistant clones, with varying probabilities of recurrence (39–41). This is particularly evident among patients with partial GTV failure, where areas of S-GTV showed higher increases in ADC values at all time points compared to their R-GTV counterparts. These subregions share

the same baseline clinical features and serve as internal controls, thereby, strengthening our data. Notably, the magnitude of ADC change among sensitive versus resistant GTV regions was consistent and independent of the patterns of failure, regardless of whether measured in patients with entire, partial, or no GTV recurrence (Figure 2C and Supplementary Figure 2). This consistency underscores the potential of ADC change as a reproducible imaging biomarker for assessing treatment response in glioblastoma. Future studies could integrate spatial transcriptomics with longitudinal functional imaging to map gene expression patterns in regions of radioresponse and resistance. This could enable personalized radiotherapy strategies tailored to each tumour's unique gene expression and response profile, such as "dose painting", which involves prescribing different radiation doses to radiosensitive and radioresistant regions.

Our study has several strengths, including the use of uniform DWI protocols and the prospective acquisition of MRI at predefined time points, which allowed for reliable comparisons. Moreover, to ensure that regions labeled S-GTV truly represent areas of responsive tumour, we included patients whose S-GTV remained free of recurrence until the last follow-up and who were followed for a minimum of 14 months (partial GTV failure) or 20 months (no GTV failure), which is significantly longer than the expected median progression-free survival for this population (~7 months)(42). The limitations include the small number of patients with partial and no GTV failure, the lack of internal and external validation, and the possibility that dynamic anatomical changes may have led to instances of image misregistration. To mitigate misregistration bias, we contoured individual GTVs at each time point (Fx0, Fx10, Fx20, P1M) and excluded patients with relevant tumour or cavity migration upon visual inspection. Given the substantial differences in ADC changes between R-GTV and S-GTV across all cohorts, and the observation that individual patient analysis showed the expected ADC changes in all but one

patient with partial failure, it is unlikely that our results were influenced by registration errors. However the accuracy of our findings could be further improved by using more sophisticated registration tools, which we plan to investigate in future studies.

Our future research will focus on identifying the optimal threshold of ADC changes at Fx10 and Fx20 for predicting geographical recurrence and validating our findings in separate cohorts of patients treated on the MR-Linac (xxxxxx, xxxxxx, xxxxxx)(21). This will be crucial for assessing the generalizability and reproducibility of our data. Additionally, we aim to investigate whether incorporating other functional sequences can improve spatial recurrence prediction over DWI alone (43–45), and to study functional MRI signal changes in the peritumoural region to predict early white matter infiltration, potentially guiding personalized FLAIR contouring (46–50). These studies will be important to support the integration of serial multiparametric imaging into the design of future clinical trials of MR-guided, biologically adapted treatment strategies. Such approaches may include dose escalation in non-responsive GTV sub-volumes attempting at improving tumour control and/or de-escalation in responsive regions to reduce toxicity and enhance quality of life.

In conclusion, early ADC changes during radiotherapy are promising imaging biomarkers for spatial tumour response and recurrence prediction in glioblastoma. GTV regions exhibiting smaller ADC changes during chemoradiation indicate potential sites of recurrence, suggesting the utility of serial DWI for designing MR-guided, biologically adapted dose-escalation clinical trials. Our data provide a foundation for replicating similar methodologies in other clinical scenarios and may inform adaptive treatment strategies across various tumour sites. Our future research will focus on determining optimal ADC change thresholds for geographical recurrence

prediction and validating these findings in independent cohorts of patients treated with daily MR-guided radiotherapy (xxxxxx, xxxxxx, xxxxxx)(21).

References

1. Ostrom QT, Price M, Neff C, Cioffi G, Waite KA, Kruchko C, et al. CBTRUS Statistical Report: Primary Brain and Other Central Nervous System Tumors Diagnosed in the United States in 2015–2019. Neuro-Oncol. 2022 Oct 5;24(Supplement_5):v1–95.

2. Minniti G, Tini P, Giraffa M, Capone L, Raza G, Russo I, et al. Feasibility of clinical target volume reduction for glioblastoma treated with standard chemoradiation based on patterns of failure analysis. Radiother Oncol. 2023 Apr;181:109435.

3. Souhami L, Seiferheld W, Brachman D, Podgorsak EB, Werner-Wasik M, Lustig R, et al. Randomized comparison of stereotactic radiosurgery followed by conventional radiotherapy with carmustine to conventional radiotherapy with carmustine for patients with glioblastoma multiforme: Report of Radiation Therapy Oncology Group 93-05 protocol. Int J Radiat Oncol. 2004 Nov;60(3):853–60.

4. Cardinale R, Won M, Choucair A, Gillin M, Chakravarti A, Schultz C, et al. A phase II trial of accelerated radiotherapy using weekly stereotactic conformal boost for supratentorial glioblastoma multiforme: RTOG 0023. Int J Radiat Oncol. 2006 Aug;65(5):1422–8.

5. Omuro A, Beal K, Gutin P, Karimi S, Correa DD, Kaley TJ, et al. Phase II Study of Bevacizumab, Temozolomide, and Hypofractionated Stereotactic Radiotherapy for Newly Diagnosed Glioblastoma. Clin Cancer Res. 2014 Oct 1;20(19):5023–31.

6. Mallick S, Kunhiparambath H, Gupta S, Benson R, Sharma S, Laviraj MA, et al. Hypofractionated accelerated radiotherapy (HART) with concurrent and adjuvant temozolomide in newly diagnosed glioblastoma: a phase II randomized trial (HART-GBM trial). J Neurooncol. 2018 Oct;140(1):75–82.

7. Gondi V, Pugh S, Tsien C, Chenevert T, Gilbert M, Omuro A, et al. Radiotherapy (RT) Dose-intensification (DI) Using Intensity-modulated RT (IMRT) versus Standard-dose (SD) RT with Temozolomide (TMZ) in Newly Diagnosed Glioblastoma (GBM): Preliminary Results of NRG Oncology BN001. Int J Radiat Oncol. 2020 Nov;108(3):S22–3.

8. Piroth MD, Pinkawa M, Holy R, Klotz J, Schaar S, Stoffels G, et al. Integrated boost IMRT with FET-PET-adapted local dose escalation in glioblastomas: Results of a prospective phase II study. Strahlenther Onkol. 2012 Apr;188(4):334–9.

9. Vora SA, Pafundi D, DeWees TA, Voss M, Ashman JB, Bendock B, et al. Phase II study of short course hypofractionated proton beam therapy incorporating 18F-DOPA-PET/MRI for elderly patients with newly diagnosed glioblastoma. J Clin Oncol. 2023 Jun 1;41(16_suppl):2002–2002.

10. Laprie A, Noel G, Chaltiel L, Truc G, Sunyach MP, Charissoux M, et al. Randomized phase III trial of metabolic imaging-guided dose escalation of radio-chemotherapy in patients with newly diagnosed glioblastoma (SPECTRO GLIO trial). Neuro-Oncol. 2024 Jan 5;26(1):153–63.

11. Einstein DB, Wessels B, Bangert B, Fu P, Nelson AD, Cohen M, et al. Phase II Trial of Radiosurgery to Magnetic Resonance Spectroscopy–Defined High-Risk Tumor Volumes in Patients With Glioblastoma Multiforme. Int J Radiat Oncol. 2012 Nov;84(3):668–74.

12. Kim MM, Sun Y, Aryal MP, Parmar HA, Piert M, Rosen B, et al. A Phase 2 Study of Dose-intensified Chemoradiation Using Biologically Based Target Volume Definition in Patients With Newly Diagnosed Glioblastoma. Int J Radiat Oncol. 2021 Jul;110(3):792–803.

13. Laack NN, Pafundi D, Anderson SK, Kaufmann T, Lowe V, Hunt C, et al. Initial Results of a Phase 2 Trial of 18F-DOPA PET-Guided Dose-Escalated Radiation Therapy for Glioblastoma. Int J Radiat Oncol. 2021 Aug;110(5):1383–95.

14. Douglas JG, Stelzer KJ, Mankoff DA, Tralins KS, Krohn KA, Muzi M, et al. [F-18]-fluorodeoxyglucose positron emission tomography for targeting radiation dose escalation for patients with glioblastoma multiforme: Clinical outcomes and patterns of failure. Int J Radiat Oncol. 2006 Mar;64(3):886–91.

15. Pramanik PP, Parmar HA, Mammoser AG, Junck LR, Kim MM, Tsien CI, et al. Hypercellularity Components of Glioblastoma Identified by High b-Value Diffusion-Weighted Imaging. Int J Radiat Oncol. 2015 Jul;92(4):811–9.

16. Wahl DR, Kim MM, Aryal MP, Hartman H, Lawrence TS, Schipper MJ, et al. Combining Perfusion and High B-value Diffusion MRI to Inform Prognosis and Predict Failure Patterns in Glioblastoma. Int J Radiat Oncol. 2018 Nov;102(4):757–64.

17. Elson A, Paulson E, Bovi J, Siker M, Schultz C, Laviolette PS. Evaluation of pre-radiotherapy apparent diffusion coefficient (ADC): patterns of recurrence and survival outcomes analysis in patients treated for glioblastoma multiforme. J Neurooncol. 2015 May;123(1):179–88.

18. xxxxx

19. xxxxx

20. xxxxx

21. xxxxx

22. Chenevert TL. Diffusion Magnetic Resonance Imaging: an Early Surrogate Marker of Therapeutic Efficacy in Brain Tumors. J Natl Cancer Inst. 2000 Dec 20;92(24):2029–36.

23. Sugahara T, Korogi Y, Kochi M, Ikushima I, Shigematu Y, Hirai T, et al. Usefulness of diffusion-weighted MRI with echo-planar technique in the evaluation of cellularity in gliomas. J Magn Reson Imaging. 1999 Jan;9(1):53–60.

24. Lawrence LSP, Chan RW, Chen H, Keller B, Stewart J, Ruschin M, et al. Accuracy and precision of apparent diffusion coefficient measurements on a 1.5 T MR-Linac in central nervous system tumour patients. Radiother Oncol. 2021 Nov;164:155–62.

25. Ellingson BM, Malkin MG, Rand SD, Connelly JM, Quinsey C, LaViolette PS, et al. Validation of functional diffusion maps (fDMs) as a biomarker for human glioma cellularity. J Magn Reson Imaging. 2010 Mar;31(3):538–48.

26. Eidel O, Neumann JO, Burth S, Kieslich PJ, Jungk C, Sahm F, et al. Automatic Analysis of Cellularity in Glioblastoma and Correlation with ADC Using Trajectory Analysis and Automatic Nuclei Counting. Najbauer J, editor. PLOS ONE. 2016 Jul 28;11(7):e0160250.

27. Park JE, Kim HS, Kim N, Park SY, Kim YH, Kim JH. Spatiotemporal Heterogeneity in Multiparametric Physiologic MRI Is Associated with Patient Outcomes in IDH-Wildtype Glioblastoma. Clin Cancer Res. 2021 Jan 1;27(1):237–45.

28. Ellingson BM, Cloughesy TF, Lai A, Nghiemphu PL, Liau LM, Pope WB. Quantitative probabilistic functional diffusion mapping in newly diagnosed glioblastoma treated with radiochemotherapy. Neuro-Oncol. 2013 Mar 1;15(3):382–90.

29. Hamstra DA, Galbán CJ, Meyer CR, Johnson TD, Sundgren PC, Tsien C, et al. Functional Diffusion Map As an Early Imaging Biomarker for High-Grade Glioma: Correlation With Conventional Radiologic Response and Overall Survival. J Clin Oncol. 2008 Jul 10;26(20):3387–94.

30. Chenevert T, Malyarenko D, Galbán C, Gomez-Hassan D, Sundgren P, Tsien C, et al. Comparison of Voxel-Wise and Histogram Analyses of Glioma ADC Maps for Prediction of Early Therapeutic Change. Tomography. 2019 Mar 1;5(1):7–14.

31. xxxxx

32. Tseng CL, Stewart J, Whitfield G, Verhoeff JJC, Bovi J, Soliman H, et al. Glioma consensus contouring recommendations from a MR-Linac International Consortium Research Group and evaluation of a CT-MRI and MRI-only workflow. J Neurooncol. 2020 Sep;149(2):305–14.

33. Wen PY, Van Den Bent M, Youssef G, Cloughesy TF, Ellingson BM, Weller M, et al. RANO 2.0: Update to the Response Assessment in Neuro-Oncology Criteria for High- and Low-Grade Gliomas in Adults. J Clin Oncol. 2023 Nov 20;41(33):5187–99.

34. Jenkinson M, Smith S. A global optimisation method for robust affine registration of brain images. Med Image Anal. 2001 Jun;5(2):143–56.

35. Jenkinson M, Bannister P, Brady M, Smith S. Improved Optimization for the Robust and Accurate Linear Registration and Motion Correction of Brain Images. NeuroImage. 2002 Oct;17(2):825–41.

36. Venables WN, Ripley BD, Venables WN. Modern applied statistics with S. 4th ed. New York: Springer; 2002. 495 p. (Statistics and computing).

37. Buglione M, Pedretti S, Poliani PL, Liserre R, Gipponi S, Spena G, et al. Pattern of relapse of glioblastoma multiforme treated with radical radio-chemotherapy: Could a margin reduction be proposed? J Neurooncol. 2016 Jun;128(2):303–12.

38. Mohamed ASR, Abusaif A, He R, Wahid KA, Salama V, Youssef S, et al. Prospective validation of diffusion-weighted MRI as a biomarker of tumor response and oncologic outcomes in head and neck cancer: Results from an observational biomarker pre-qualification study. Radiother Oncol. 2023 Jun;183:109641.

39. Greenwald AC, Darnell NG, Hoefflin R, Simkin D, Mount CW, Gonzalez Castro LN, et al. Integrative spatial analysis reveals a multi-layered organization of glioblastoma. Cell. 2024 May;187(10):2485-2501.e26.

40. Mathur R, Wang Q, Schupp PG, Nikolic A, Hilz S, Hong C, et al. Glioblastoma evolution and heterogeneity from a 3D whole-tumor perspective. Cell. 2024 Jan;187(2):446-463.e16.

41. Shireman JM, Cheng L, Goel A, Garcia DM, Partha S, Quiñones-Hinojosa A, et al. Spatial transcriptomics in glioblastoma: is knowing the right zip code the key to the next therapeutic breakthrough? Front Oncol. 2023 Oct 17;13:1266397.

42. Stupp R, Mason WP, van den Bent MJ, Weller M, Fisher B, Taphoorn MJB, et al. Radiotherapy plus Concomitant and Adjuvant Temozolomide for Glioblastoma. N Engl J Med. 2005 Mar 10;352(10):987–96.

43. Mehrabian H, Myrehaug S, Soliman H, Sahgal A, Stanisz GJ. Evaluation of Glioblastoma Response to Therapy With Chemical Exchange Saturation Transfer. Int J Radiat Oncol. 2018 Jul;101(3):713–23.

44. Chan RW, Lawrence LSP, Oglesby RT, Chen H, Stewart J, Theriault A, et al. Chemical exchange saturation transfer MRI in central nervous system tumours on a 1.5 T MR-Linac. Radiother Oncol. 2021 Sep;162:140–9.

45. Mehrabian H, Myrehaug S, Soliman H, Sahgal A, Stanisz GJ. Quantitative Magnetization Transfer in Monitoring Glioblastoma (GBM) Response to Therapy. Sci Rep. 2018 Feb 6;8(1):2475.

46. Gupta A, Young RJ, Karimi S, Sood S, Zhang Z, Mo Q, et al. Isolated Diffusion Restriction Precedes the Development of Enhancing Tumor in a Subset of Patients with Glioblastoma. Am J Neuroradiol. 2011 Aug;32(7):1301–6.

47. Matsuda K, Kokubo Y, Kanemura Y, Kanoto M, Sonoda Y. Preoperative Apparent Diffusion Coefficient of Peritumoral Lesion Associate with Recurrence in Patients with Glioblastoma. Neurol Med Chir (Tokyo). 2022;62(1):28–34.

48. Chang PD, Chow DS, Yang PH, Filippi CG, Lignelli A. Predicting Glioblastoma Recurrence by Early Changes in the Apparent Diffusion Coefficient Value and Signal Intensity on FLAIR Images. Am J Roentgenol. 2017 Jan;208(1):57–65.

49. Chen LL, Ulmer S, Deisboeck TS. An agent-based model identifies MRI regions of probable tumor invasion in a patient with glioblastoma. Phys Med Biol. 2010 Jan 21;55(2):329–38.

50. Akbari H, Macyszyn L, Da X, Bilello M, Wolf RL, Martinez-Lage M, et al. Imaging Surrogates of Infiltration Obtained Via Multiparametric Imaging Pattern Analysis Predict Subsequent Location of Recurrence of Glioblastoma. Neurosurgery. 2016 Apr;78(4):572–80.

Supplementary Table 1: Diffusion-weighted imaging (DWI) protocols by scanner: DWI was acquired on all scanners with single-shot echo planar imaging readout. The acquisition voxel size is listed, as opposed to the reconstructed size. The number of averages is shown in brackets next to each b-value. The protocol on the 1.5T Ingenia was updated partway through the study.

Supplementary Table 2: Multivariable analyses for predictors of GTV recurrence

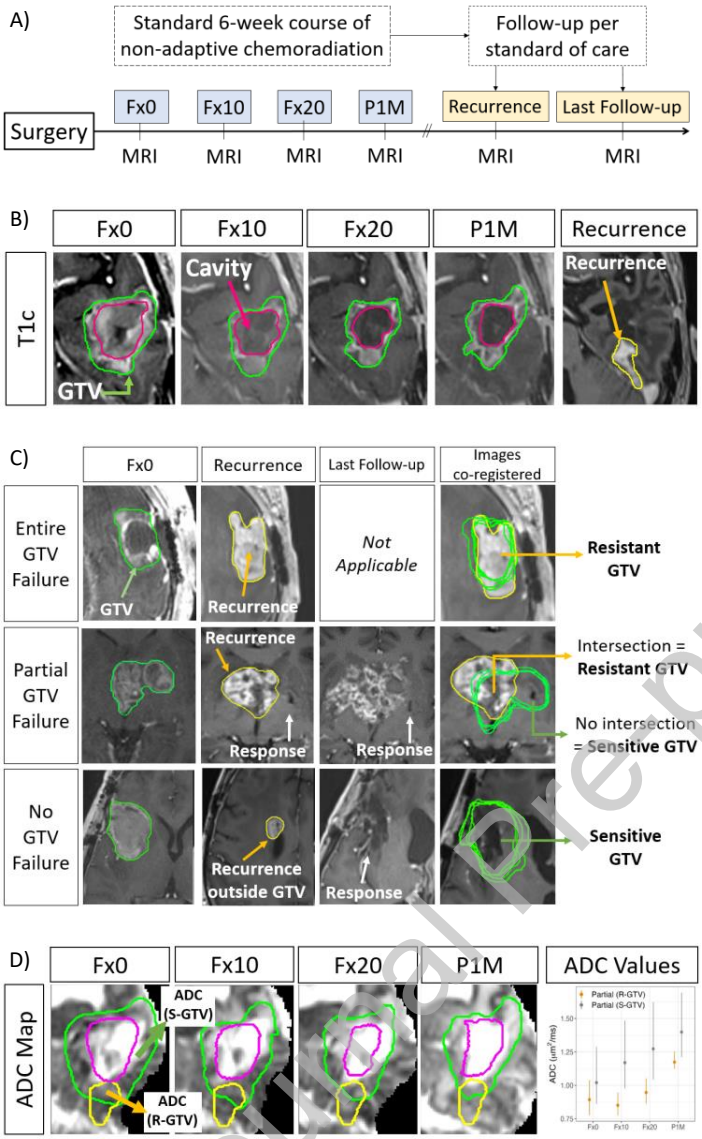

Figures

Figure 1: Methodology Overview. A) In this prospective observational study, patients underwent multiparametric MRI at radiotherapy planning (baseline, Fx0), fraction 10 (Fx10), fraction 20 (Fx20), and one month after completing a standard non-adaptive 6-week course of concurrent chemoradiation (P1M). Follow-up was conducted according to standard care. **B)** The GTV and the interior of the surgical cavity were contoured at the aforementioned time points

(Fx0, Fx10, Fx20, P1M). Contrast-enhancing recurrence was contoured at the first MRI showing progression per RANO 2.0 criteria. **C)** The region of interest was defined according to the pattern of GTV failure. Patients were classified as having "entire GTV failure", "partial GTV failure" (part of the GTV recurred, while another sub-volume remained recurrence-free until the last follow-up), or "no GTV failure" (no recurrence in the GTV until the last follow-up). For patients with entire GTV failure, the entire GTV was labeled Resistant-GTV. For those with partial GTV failure, the GTV region intersecting with the recurrence was labeled Resistant-GTV, while the region not intersecting was labeled Sensitive-GTV. For patients with no GTV failure, the entire GTV was labeled Sensitive-GTV. **D)** ADC values and percentage changes from baseline were compared between Resistant-GTV and Sensitive-GTV at each time point. The surgical cavity was excluded from ADC measurements to avoid bias.

Abbreviation: ADC, apparent diffusion coefficient; Fx0, Fraction 0; Fx10, Fraction10; Fx20, Fraction 20; P1M, 1 month post-treatment; GTV, gross tumour volume; MRI, magnetic resonance imaging; T1c, T1-weighted contrast-enhanced magnetic resonance imaging.

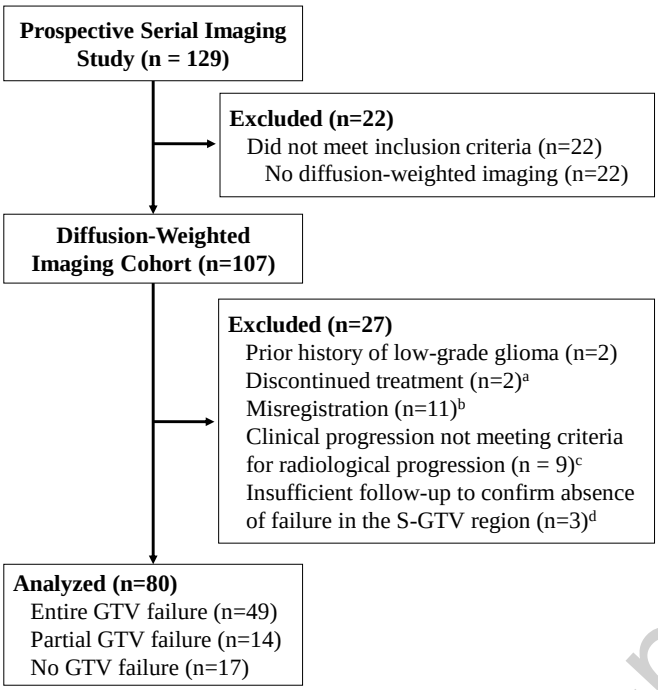

Figure 2: CONSORT diagram

Abbreviation: GTV, gross tumour volume; S-GTV, sensitive-gross tumour volume.

[a] One patient with a solid-cystic lesion required reoperation and Ommaya reservoir placement due to cyst expansion during the second week of radiation; one patient experienced clinical deterioration, leading to treatment discontinuation, with no further imaging or clinical follow-up.[b] The main cause of misregistration was significant GTV dynamics, mainly cavity shrinkage, which altered GTV volume and shape, leading to inaccurate coregistration.

[c] Upon clinical deterioration, three patients received bevacizumab for presumed disease progression versus radiation necrosis; one underwent resection for presumed radiation necrosis, with pathology revealing glioblastoma with extensive necrosis, leaving uncertainty about true

progression versus radiation necrosis; and five patients experienced clinical decline without subsequent follow-up imaging.

[d] Three patients died of distant progression within one year of treatment without GTV recurrence. Due to their limited follow-up, it is unclear whether they might have later recurred in the S-GTV region had they survived longer, leaving uncertainty about whether these areas were truly radiosensitive.

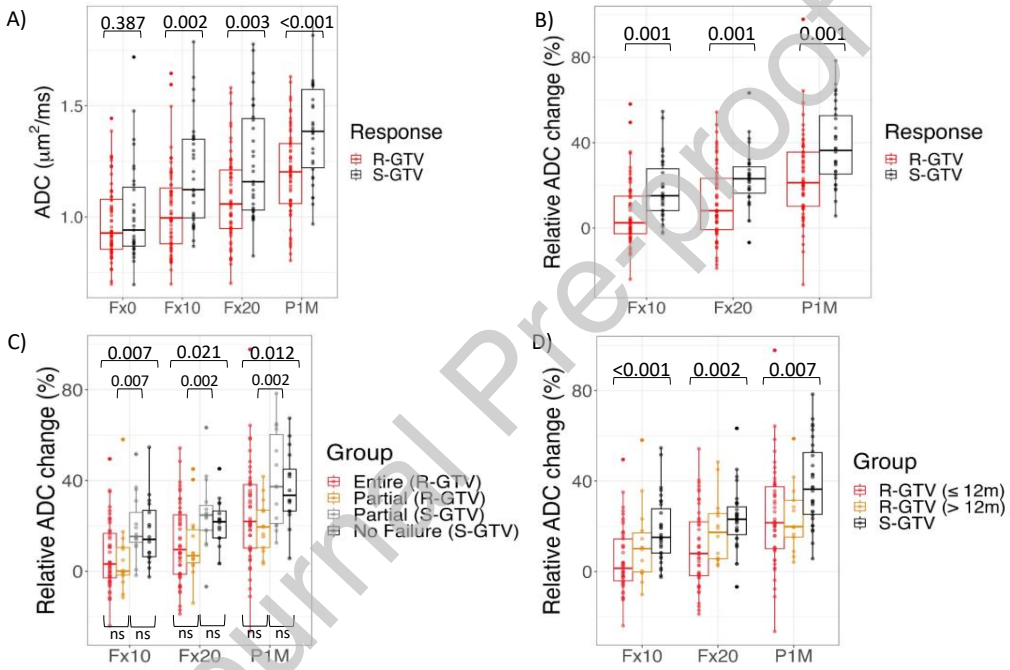

Figure 3: Absolute ADC Values and Relative Changes from Baseline at Various Time Points. A) Absolute ADC values within resistant and sensitive GTV. **B**) Relative ADC changes within resistant and sensitive GTV. **C**) ADC changes stratified by the pattern of GTV failure. **D**) ADC changes stratified by the time to GTV failure.

P-values were reported for each comparison and calculated using the following statistical tests: **A)** unpaired two-sided t-test; **B)** unpaired two-sided t-test; **C)** paired two-sided t-test compared

R-GTV and S-GTV sub-volumes within the partial GTV failure cohort (same patients), and an unpaired two-sided t-test compared ADC changes between the entire GTV failure and partial GTV failure (R-GTV sub-volume) or between no GTV failure and partial GTV failure (S-GTV sub-volume); **D)** one-way analysis of variance (ANOVA). Abbreviation: ADC, apparent diffusion coefficient; Fx0, Fraction 0; Fx10, Fraction10; Fx20, Fraction 20; P1M, 1 month post-treatment; ns, non-significant p-value; R-GTV, resistant-gross tumour volume; S-GTV, sensitive-gross tumour volume.

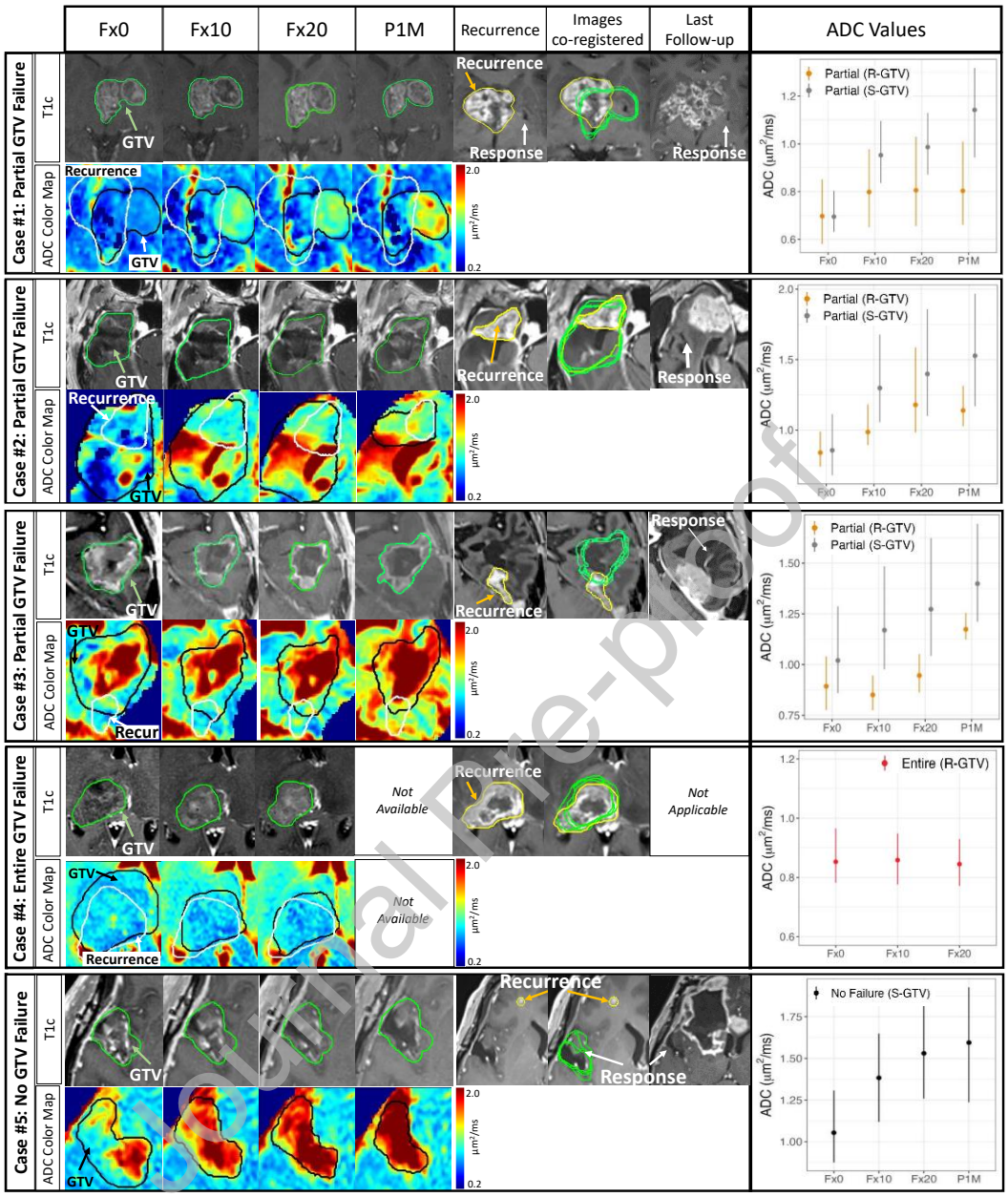

Figure 4: Examples of Temporal ADC Changes across Different Patterns of GTV Failure. The graphs present absolute ADC values at various time points, enabling quantitative comparison, while the ADC color maps provide intuitive visualization of spatial heterogeneity in tumour response. **Case #1**: 22-year-old patient with basal ganglia IDH wildtype glioblastoma, MGMT unmethylated, post-biopsy, treated with 60 Gy/30 fractions. One tumour focus

responded completely to treatment, while another progressed after 12 months. The patient died 15 months post-treatment. **Case #2**: 68-year-old patient with temporal IDH wildtype glioblastoma, MGMT methylated, post-gross total resection, treated with 60 Gy/30 fractions. Recurrence occurred in part of the surgical cavity 4 months post-treatment, and the patient died after 13 months. **Case #3**: 65-year-old patient with temporal IDH wildtype glioblastoma, MGMT methylated, post-subtotal resection, treated with 60 Gy/30 fractions. Recurrence occurred in part of the surgical cavity 44 months post-treatment, and the patient is alive after 57 months of follow-up. In **cases #1-3**, progression occurred in GTV areas with smaller ADC increases during radiation, suggesting that less tumour cell kill in these regions ultimately led to tumour recurrence. The areas labeled S-GTV remained recurrence-free until the last follow-up. **Case #4**: 39-year-old patient with thalamus IDH wildtype glioblastoma, MGMT methylated, post-biopsy, treated with 54 Gy/30 fractions. The entire tumour had stable ADC values throughout treatment and progressed after 4 months. The patient died after 9 months. **Case #5**: 51-year-old patient with temporal IDH wildtype glioblastoma, MGMT methylated, post-gross total resection, treated with 60 Gy/30 fractions. Progression outside the CTV occurred 26 months post-treatment. A significant increase in ADC values was observed in the GTV, which remained free of recurrence for 37 months, when the patient died. In all cases, the GTV was represented in green (T1-weighted MRI) or in black (ADC color map), while the recurrence was represented in yellow (T1-weighted MRI) or in white (ADC color map).

Abbreviation: ADC, apparent diffusion coefficient; Fx0, Fraction 0; Fx10, Fraction10; Fx20, Fraction 20; P1M, 1 month post-treatment; GTV, gross tumour volume; R-GTV, resistant-gross tumour volume; S-GTV, sensitive-gross tumour volume; T1c, T1-weighted contrast-enhanced magnetic resonance imaging.

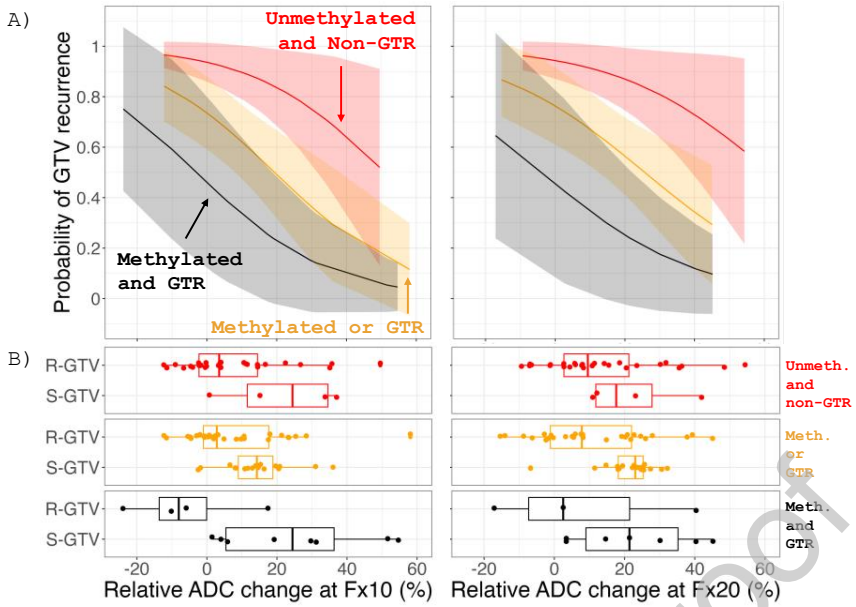

Figure 5: ADC change relative to baseline is an independent predictor of GTV recurrence. **A)** Logistic regression modeling of the probability of GTV recurrence as a function of MGMT promotor methylation status, extent of surgical resection, and ADC change at fractions 10 and 20 relative to pre-treatment. Increasing ADC change predicts lower probability of recurrence. Colours indicate MGMT methylation status and extent of surgical resection. The shaded regions indicate the 95% confidence interval. **B)** Individual measurements used to fit the logistic regression model. Each panel shows a different combination of MGMT methylation status and extent of surgical resection.

Abbreviation: ADC, apparent diffusion coefficient; Fx10, Fraction 10; Fx20, Fraction 20; GTR, gross tumour resection; MGMT, Methylguanine-DNA methyltransferase promoter methylation status; unmeth, unmethylated; Meth, methylated; R-GTV, resistant-gross tumour volume; S-GTV, sensitive-gross tumour volume

Supplementary Figure 1: Realative ADC change stratified by the pattern of failure and tumour response. A) Relative ADC change for resistant-GTVs according to the pattern of failure. **B)** Relative ADC changes for partial GTV failure cohort according to tumour response. **C)** Relative ADC change for sensitive-GTVs according to the pattern of failure.

Abbreviation: ADC, apparent diffusion coefficient; Fx0, Fraction 0; Fx10, Fraction10; Fx20, Fraction 20; P1M, 1 month post-treatment; R-GTV, resistant-gross tumour volume; S-GTV, sensitive-gross tumour volume.

Supplementary Figure 2: Relative ADC Changes From Baseline for Each Patient with Partial GTV Failure

Fraction 0 (Fx0) corresponds to week -1, fraction 10 (Fx10) to week 2, fraction 20 (Fx20) to week 4, and 1 month post-treatment (P1M) to week 10.

Abbreviation: ADC, apparent diffusion coefficient; R-GTV, resistant-gross tumour volume; S-GTV, sensitive-gross tumour volume.

Supplementary Figure 3: Baseline Absolute ADC Values Stratified by Extent of Surgical Resection

Abbreviation: ADC, apparent diffusion coefficient; Fx0, GTR, gross tumour resection, STR, Subtotal resection; Min, minimum; Max, maximum; IQR, interquartile range

Table 1. Patient, tumor, and treatment characteristics for the entire cohort and stratified by the pattern of GTV failure.

: Patient, tumour, and treatment characteristics for the entire cohort and stratified by the pattern of GTV failure.

		Cohorts			
Parameter	Total (n=80)	Entire GTV Failure (n=49)	Partial GTV Failure (n=14)	No GTV Failure (n=17)	P value[a]
Sex					0.305
Male	52 (65)	32 (65)	7 (50)	13 (76)	
Female	28 (35)	17 (35)	7 (50)	4 (24)	
Age, years	54 (19-75)	56 (19-75)	56 (22-68)	51 (22-69)	0.300
ECOG					0.360
0-1	60 (75)	33 (67)	12 (86)	15 (88)	
2	18 (23)	14 (0)	2 (14)	2 (12)	
3	2 (3)	2 (4)	0 (0)	0 (0)	
Tumour Location					0.363
Thalamus/Brainstem	10 (13)	9 (18)	1 (7)	0 (0)	
Frontal	23 (29)	13 (27)	6 (43)	4 (24)	
Parietal	16 (20)	11 (22)	2 (14)	3 (18)	
Temporal	30 (38)	15 (31)	5 (36)	10 (59)	
Cerebellum	1 (1)	1 (1)	0 (0)	0 (0)	
Extent of resection					**0.049**
Biopsy	13 (16)	12 (24)	1 (7)	0 (0)	
STR	43 (54)	27 (55)	7 (50)	9 (53)	
GTR	24 (30)	10 (20)	6 (43)	8 (47)	
IDH mutation status					0.138
Mutant	3 (4)	1 (2)	0 (0)	2 (12)	
Wildtype	77 (96)	48 (98)	14 (100)	15 (88)	
MGMT promoter methylation status					**0.005**
Methylated	34 (43)	14 (29)	8 (57)	12 (71)	
Unmethylated	42 (53)	32 (65)	6 (43)	4 (24)	
Indeterminate	4 (5)	3 (6)	0 (0)	1 (6)	
GTV at baseline (Fx0, cc)	18.6 (2.4-97.0)	19.8 (2.4-97.0)	19.0 (6.6-76.1)	11.1 (3.1-47.8)	0.173
Radiotherapy dose					0.176
60 Gy/30 Fx	64 (80)	36 (73)	13 (93)	15 (88)	
54-56 Gy/27-30 Fx	16 (20)	13 (27)	1 (7)	2 (12)	
Completed Adjuvant Temozolomide	45 (56)	18 (37)	11 (79)	16 (94)	**<0.001**
Follow-up, months	48.4 (4.3-64.5)	19.9 (4.3-59.6)	48.4 (14.4-58.1)	44.5 (20.8-64.5)	

Categorical data is presented as n (%) and continuous as median (range)

a Chi-square test (categorical) or ANOVA (continuous)

Graphical Abstract